Available online at www.sciencedirect.com
ScienceDirect
Journal of Solid State Chemistry 181 (2008) 1110–1115
JOURNAL OF SOLID STATE CHEMISTRY
www.elsevier.com/locate/jssc

Chirality and ferromagnetism in $NiBPO_4(OH)_2$ containing helix edge-sharing NiO_6 chains

Tao Yang[a], Jing Ju[b], Fuhui Liao[a], Juns Sasaki[b], Naoki Toyota[b], Jianhua Lin[a,*]

[a]*Beijing National Laboratory for Molecular Sciences, State Key Laboratory for Rare Earth Materials Chemistry and Applications, College of Chemistry and Molecular Engineering, Peking University, Beijing 100871, China*
[b]*Physics Department, Graduate School of Science, Tohoku University, Sendai 980-8578, Japan*

Received 13 November 2007; received in revised form 25 January 2008; accepted 28 January 2008
Available online 10 March 2008

Abstract

Two isotypic borophosphates $MBPO_4(OH)_2$ (M = Mg, Ni) have been hydrothermally synthesized and structurally characterized by powder X-ray diffraction in the space group $P3_121$. Nickel (or magnesium) atoms are octahedrally coordinated. The octahedra share edges to form helix chains around the three-fold screw-axis. Boron and phosphorus atoms are both tetrahedrally coordinated. The BO_4 and PO_4 tetrahedra are alternately connected, forming vierer-single chains. These two kinds of chains are intersected in the three-dimensional framework structure. $NiBPO_4(OH)_2$ can be considered as a quasi-one-dimensional magnet because the shortest Ni^{2+}–Ni^{2+} distance within the helix chain is about 3.187(1) Å, while the shortest inter-chain connection of the nickel ions is through a BO_4 group (5.650(1) Å). Both dc and alternating current (ac) susceptibilities and isothermal magnetization have been measured on powder sample. The intra- and inter-chain interactions are proved to be both ferromagnetic, and a long-range ordering is established below 2.2 K in $NiBPO_4(OH)_2$.

Keywords: Chiral; Ferromagnetism; Nickel; Magnesium; Borophosphate

1. Introduction

Solid-state compounds with chiral structures are well known to exhibit optical activity and have been the interest of research efforts for many years. Recently, attention has been focused on magnetic materials with chiral structures because they may exhibit magnetochiral dichroic (MChD) effect, a phenomenon observed by Rikken and Raupach [1] on luminescent spectrum of a chiral complex, Tris(3-trifluoroacetyl-±-camphorato) europium(III). Although a number of chiral magnetic materials have been studied, their MChD effects are all relatively weak [1–4]. A notable fact is that the materials studied in this category so far are mainly molecular-based materials. This is understandable because the design and preparation of the chiral structures may be much easily envisioned by choosing, for example, chiral ligands and magnetic active metal ions. The MChD effect is associated with chirality and magnetic ordering. Thus transition metal oxides may have less chance because only few may crystallize in chiral structures, although many of them exhibit strong magnetic interactions. The borophosphates possess complicated linkages of triangular BO_3 and tetrahedral BO_4 and PO_4 and appear with abundant different structure types, which often crystallize in non-centrosymmetric or even chiral symmetry [5,6]. In fact, solid-state borophosphates might be a large resource for the optical active and electro-optical active materials due to the rich complexity in crystal structure.

In most of the borophosphates, the polyhedra of the metal ions tend to be distributed in the borate or borophosphate matrix in order to avoid the accumulation of the local charges; therefore, the metal ions often appear as isolated [7–28] or oligomeric [29–41] polyhedra. For example, one could refer $M^{I}M^{II}(H_2O)_2[BP_2O_8]\cdot nH_2O$ (M^{I} = NH^{4+}, Li–K; M^{II} = Mg, Mn–Zn) [7–15] and $Na_2[M^{II}B_3P_2O_{11}(OH)]\cdot 0.67H_2O$ (M^{II} = Mg, Mn–Zn) [16–18];

*Corresponding author. Fax: +86 10 6275 1708.
E-mail address: jhlin@pku.edu.cn (J. Lin).

0022-4596/$ - see front matter © 2008 Elsevier Inc. All rights reserved.
doi:10.1016/j.jssc.2008.01.048

both structures crystallize in chiral space groups, but the transition metal ions are well separated by borate and phosphate groups; therefore no long-range magnetic ordering is observed because of the poor super-exchange interactions via three-atom bridges (i.e. O–B–O or O–P–O). One exceptional case is $[NH_4]_4[Mn_9B_2(OH)_2(HPO_4)_4(PO_4)_6]$, which features anionic manganese–phosphate double layers $[Mn_9(OH)_2(HPO_4)_4(PO_4)_6]^{10-}$ composed of MnO_5, MnO_6, PO_4 and HPO_4 polyhedral units [42]. It shows a long-range spin canted antiferromagnetic (AFM) ordering below 8.0 K originated from the infinite Mn–O–Mn layers. However, the multiple magnetic pathways in this structure make the extraction of coupling parameters impossible. Recently, a series of isotypic borophosphates $MBPO_4(OH)_2$ (M = Mn, Fe, Co) has been hydrothermally synthesized with DABCO (1,4-diazobicyclo[2.2.2]octane, $C_6H_{12}N_2$) [43]. They crystallize in the space group $P3_121$ or $P3_221$ and a notable feature of these phases is that the octahedrally coordinated metal ions share edges, forming helix chains along the c-axis. In this paper we report the synthesis of two new isotypic borophosphates $MBPO_4(OH)_2$ (M = Mg, Ni) without organic solvent. The magnetic investigation shows that $NiBPO_4(OH)_2$ can be interpreted as a quasi-one-dimensional (1D) magnet, where the intra- and inter-chain interactions are both ferromagnetic (FM), and a long-range ordering is established below 2.2 K.

2. Experimental section

2.1. Synthesis

All reagents were of analytical grade and were used as obtained from commercial sources without further purification. $MBPO_4(OH)_2$ (M = Mg, Ni) were synthesized under hydrothermal conditions. Typically, 4 mmol $Ni(CH_3COO)_2\cdot 4H_2O$ (or $Mg(NO_3)_2\cdot 6H_2O$), 20 mmol H_3BO_3 and 3 ml concentrated H_3PO_4 (14.6 mol/l) were charged into a 50 ml Teflon autoclave reactor and heated at 220 °C for 7 days. After cooling to the room temperature, the solid products were washed extensively with hot water (80 °C). The obtained Mg compound is colorless and Ni compound is yellow. Both of them are small needle-like crystals that often aggregate as balls. The typical yield is about 20% based on the metal salts.

2.2. Structure determination

Powder X-ray diffraction data for $MBPO_4(OH)_2$ (M = Mg, Ni) were collected at room temperature on a Bruker AXS D8: transmission mode, Cu $K\alpha_1$ $\lambda = 1.540596$ Å, 40 kV and 40 mA, germanium primary monochromator, PSD detector, step scan size/time: 0.0144°/40 s. The powder patterns were indexed with PowderX [44] and the possible space groups ($P3_1$ or $P3_121$) were derived from systematic absence of the reflections. The structure model was established by using a model annealing technique (TOPAS [45]) in the space group $P3_121$ and refined with the Rietveld method. During the refinement, peak shapes were modeled with the pseudo-Voigt function and a six-term Chebyshev polynomial and a $1/2\theta$ term was used to model the background. In addition, all the thermal displacement parameters of six oxygen atoms were refined equally to reduce the variables. The structure refinement also revealed about 5% BPO_4 in the powder sample, which was also taken into account in the final refinement. Fig. 1 shows the profile fitting of the Rietveld refinement for $MBPO_4(OH)_2$ (M = Mg, Ni). The crystallographic data and refined atomic parameters are also listed in Tables 1 and 2. For further details of structure study, one may refer to the deposited data from the Fachinformationszentrum Karlsruhe, 76344 Eggenstein-Leopoldshafen, Germany (fax: (+49)7247-808-666; e-mail: crysdata@fiz-karlsruhe.de), on quoting the depository numbers CSD-416089 and CSD-416129.

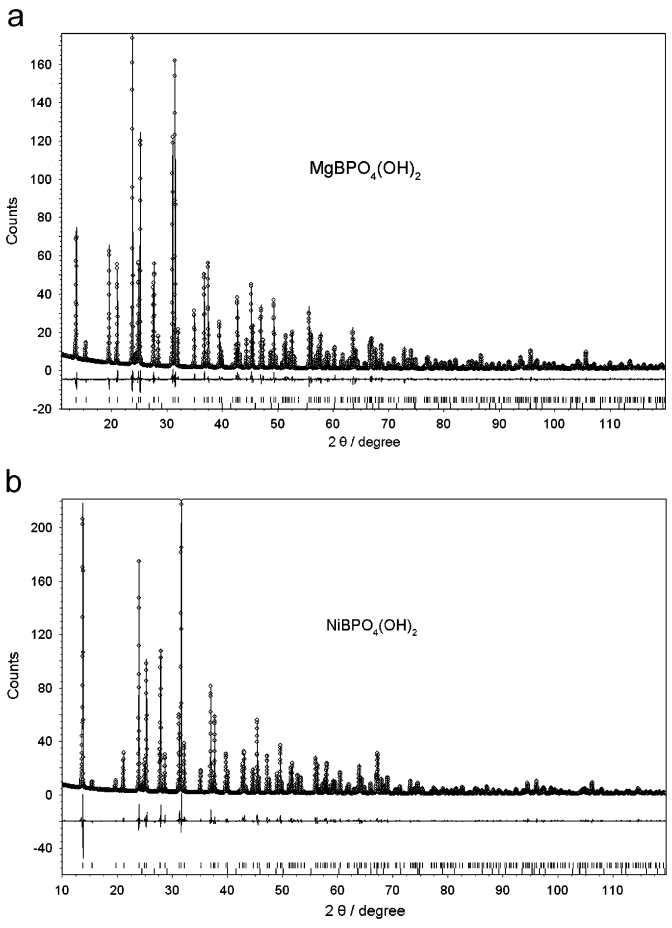

Fig. 1. Rietveld plot of the powder X-ray diffraction patterns of $MgBPO_4(OH)_2$ (a) and $NiBPO_4(OH)_2$ (b). The symbol ○ represents the observed pattern and the solid line is the calculated pattern; the marks below the diffraction patterns are the reflection positions ($MBPO_4(OH)_2$ and BPO_4), and the difference curves are also shown below the diffraction curves.

Table 1
Crystallographic data of $MBPO_4(OH)_2$ (M = Mg, Ni)

Formula	$MgBPO_4(OH)_2$	$NiBPO_4(OH)_2$
Measurement device	Bruker AXS D8	
Detector	PSD	
Monochromator	Germanium	
Collected mode	Transmission	
λ (Å)	1.540596	
Space group	$P3_121$	
Z	6	
Color	Colorless	Yellow
Formula mass	164.08	198.47
a (Å)	7.46072(3)	7.41862(3)
c (Å)	12.63283(5)	12.58982(6)
V (Å^3)	608.97(3)	600.06(1)
ρ_{calcd} (g/cm^3)	2.652	3.295
Rp	0.0527	0.0656
wRp	0.0734	0.0875

Table 2
Refined atomic parameters of (a) $MgBPO_4(OH)_2$ and (b) $NiBPO_4(OH)_2$

Atom	Site	x	y	z	U_{eq}
(a) $MgBPO_4(OH)_2$					
Mg1	3b	0.1321(3)	0.1321(3)	0.5	0.013(1)
Mg2	3a	0.2397(3)	0.2397(3)	0	0.004(1)
P	6c	0.0703(2)	0.7494(2)	0.92910(8)	0.009(1)
B	6c	0.7010(8)	0.2608(9)	0.7066(4)	0.023(3)
O1	6c	0.5524(4)	0.3384(4)	0.9806(2)	0.007(1)
O2	6c	0.2756(5)	0.7560(5)	0.8925(2)	0.007(1)
O3	6c	0.2062(5)	0.0895(4)	0.6537(2)	0.007(1)
O4	6c	0.1943(4)	0.2187(4)	0.8385(2)	0.007(1)
O5	6c	0.1684(4)	0.4159(5)	0.5504(5)	0.007(1)
O6	6c	0.3996(4)	0.4757(4)	0.6952(2)	0.007(1)
(b) $NiBPO_4(OH)_2$					
Ni1	3b	0.1330(2)	0.1330(2)	0.5	0.016(1)
Ni2	3a	0.2358(2)	0.2358(2)	0	0.011(1)
P	6c	0.0662(3)	0.7477(3)	0.9294(1)	0.013(1)
B	6c	0.697(1)	0.264(1)	0.7098(6)	0.033(1)
O1	6c	0.5521(6)	0.3371(7)	0.9821(3)	0.011(1)
O2	6c	0.2698(7)	0.7550(7)	0.8917(3)	0.011(1)
O3	6c	0.2070(7)	0.0897(6)	0.6533(3)	0.011(1)
O4	6c	0.1886(6)	0.2201(6)	0.8373(3)	0.011(1)
O5	6c	0.1696(6)	0.4197(7)	0.5445(3)	0.011(1)
O6	6c	0.3966(6)	0.4735(6)	0.6930(3)	0.011(1)

2.3. Other analyses

The dc magnetic measurements were carried out on a superconducting quantum interference device magnetometer (SQUID, Quantum Design Co.) in the temperature range 1.8–300 K. The sample was ground into fine powder and placed in a gelatin capsule fastened in a plastic straw for immersion into the SQUID. For a typical zero field cooling (ZFC) measurement, we cooled the system to 1.8 K without the external feild and then applied a 1000 Oe field, and the magnetization was measured in the following warming process. After that, we cooled the system again and measured the field cooling (FC) magnetization meanwhile. The alternating current (ac) magnetic susceptibility was measured at a 997–1003 Oe oscillating field frequency range of 10–997 Hz. The isothermal magnetization curve was measured at 1.8 K up to 7 T. The chemical analysis of metal, boron and phosphorus was conducted by inductively coupled plasma (ICP) methods on an ESCALAB2000 analyzer. The thermal stability of the sample was analyzed with thermogravimetric (TG) analysis on a Dupont 951 thermogravimetric analyzer in air with a heating rate of 10 °C/min from 30 to 800 °C. FT-IR spectroscopy was measured on a Nicolet Magna-IR-750 series II.

3. Results and discussion

3.1. Structure description

The title compounds are isostructural with $MBPO_4(OH)_2$ (M = Mn, Co, Fe) [43] and crystallize in the space group $P3_121$. Here, we describe the structure of $NiBPO_4(OH)_2$ as being representative. Two crystallographic independent metal atoms (Ni1 and Ni2) are located on two-fold axis (3b and 3a sites), and the rest of the non-hydrogen atoms, including 1 B, 1 P and 6 O, are located in general positions. Table 3 lists selected bond distances and angles, which are all regular as those in other related compounds [43]. It can be seen that the nickel atoms are both octahedrally coordinated, whereas the boron and phosphorus atoms are all tetrahedrally coordinated (BO_4 and PO_4). As shown in Fig. 2a, the NiO_6 octahedra share edges, forming helix chains along the c-axis. The BO_4 and PO_4 tetrahedra share common corners, forming borophosphate chains orientated along three equivalent directions ({100}, {010} and {110}). These two kinds of chains are interconnected, thus forming a three-dimensional (3D) framework as shown in Fig. 2b.

The bond valance sum (BVS) values calculated from the structure parameters are mostly regular ($M \approx 2$, B ≈ 3, P ≈ 5 and O ≈ 2), while O1 and O5, which are bridged to M(II) and B(III), have significant low BVS values (O1: 1.209 and O5: 1.138), implying that additional protons are bonded here. The presence of protons in the structure is supported by FT-IR and TGA experiments (see Fig. 3). Additionally, the chemical analysis of the metal, B and P elements with ICP methods (Ni:B:P = 1:1.04:0.96; Mg:B:P = 1:1.00:1.06) also agrees well with the formula $MBPO_4(OH)_2$.

3.2. Magnetic properties

The framework in $NiBPO_4(OH)_2$ is 3D; however, as far as the magnetic interactions are concerned, it can be viewed as a quasi-1D system as that in $NiH_2P_2O_7$, where the NiO_6 octahedra share edges to form zigzag chains and the chains are interconnected by P_2O_7 groups [46]. $NiH_2P_2O_7$ exhibits field-induced metamagnetic behavior due to the strong intra-chain FM and weak inter-chain antiferromagnetic

Table 3
Selected bond distances (Å) and angles (degree) of $MBPO_4(OH)_2$ (M = Mg, Ni)

Bond	$MgBPO_4(OH)_2$	$NiBPO_4(OH)_2$	Angle	$MgBPO_4(OH)_2$	$NiBPO_4(OH)_2$
$M1$–O3(×2)	2.0864(29)	2.0754(40)	O3–P–O4	113.63(13)	113.70(24)
$M1$–O5(×2)	2.0948(38)	2.0813(53)	O3–P–O6	111.94(14)	111.25(22)
$M1$–O4(×2)	2.1504(29)	2.1134(35)	O3–P–O2	110.41(20)	109.60(26)
$M2$–O4(×2)	2.0608(24)	2.0714(31)	O4–P–O6	108.74(11)	109.58(25)
$M2$–O1(×2)	2.0803(35)	2.0876(47)	O4–P–O2	105.49(12)	105.69(23)
$M2$–O3(×2)	2.1556(31)	2.1235(39)	O6–P–O2	106.16(19)	106.63(19)
P–O3	1.5068(27)	1.5026(39)	O1–B–O5	116.35(25)	116.27(32)
P–O4	1.5331(26)	1.5308(40)	O1–B–O6	112.50(46)	110.92(22)
P–O6	1.5696(31)	1.5448(41)	O1–B–O2	102.89(32)	110.00(85)
P–O2	1.5775(41)	1.5579(61)	O5–B–O6	112.11(33)	110.84(23)
B–O5	1.4097(50)	1.4429(33)	O5–B–O2	108.18(43)	103.34(19)
B–O1	1.4215(62)	1.4102(85)	O6–B–O2	103.42(19)	104.57(15)
B–O6	1.4751(65)	1.4870(49)			
B–O2	1.5509(50)	1.525(11)			

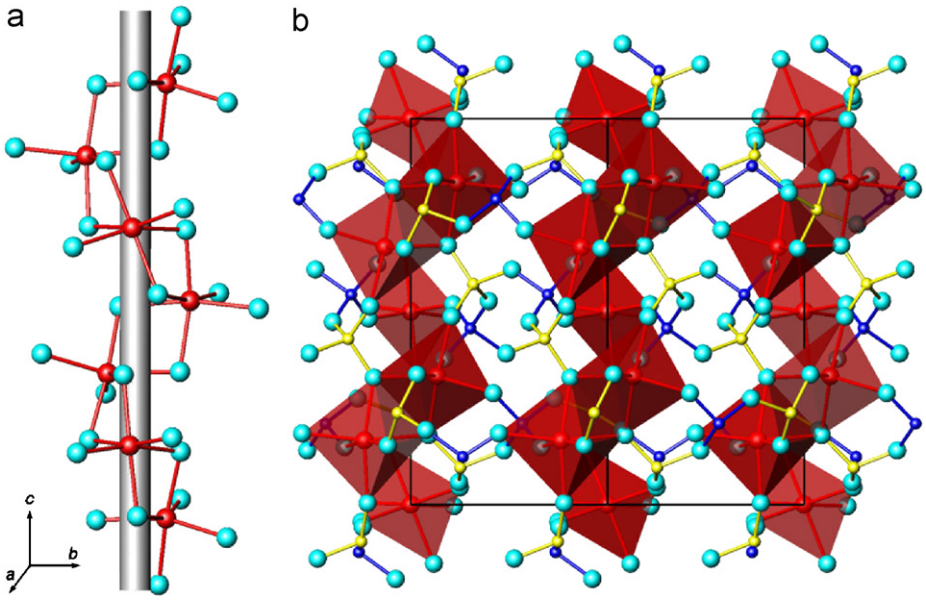

Fig. 2. (a) The NiO_6 helix chain running along the 3_1 axis. (b) The structure of $NiBPO_4(OH)_2$ viewed along the {110} direction; the NiO_6 octahedra are expressed as the red polyhedra, while the borate and phosphate groups are shown as bonded atoms: deep blue: boron; yellow: phosphorus; and cyan: oxygen.

(AFM) couplings. Here in $NiBPO_4(OH)_2$, the intra-chain metal centers are connected via double oxo-bridges with the shortest distance of 3.187(1) Å. These helix chains are well separated by borophosphate chains and the shortest inter-chain Ni^{2+}–Ni^{2+} connection is about 5.650(1) Å through O–B–O three atoms bridge. It is reasonable to assume that the main interactions between Ni^{2+} and Ni^{2+} are mediated through double oxo-bridges, while the other interactions transmitted by O–B–O or O–P–O three-atom bridges are negligible.

Dc magnetic susceptibility (χ) measurements were performed between 1.8 and 300 K on polycrystalline $NiBPO_4(OH)_2$ sample at an external field of 1000 Oe both under ZFC and FC conditions. The ZFC and FC signals are identical in the whole measured temperature region. As shown in Fig. 4a, the reciprocal susceptibility above 20 K gives a good Curie–Weiss fit with $C = 1.26\,cm^3\,K/mol$, which agrees with the expected value for isolated Ni^{2+} ions ($S = 1$). The positive value of θ (8.3 K) suggests predominant FM interactions between nickel atoms and the helix chains. Upon cooling, χ first shows a slow increase in a wide temperature region and then a very steep increase from 0.20 cm^3/mol at 12 K to 4.75 cm^3/mol at 1.8 K. Since we did not observe the saturation or maximum of the magnetic susceptibility in the measured temperature range, the inter-chain magnetic interactions are suggested to be weak, which is consistent with the former assumption. Actually, the differential of the χT curve shows a negative

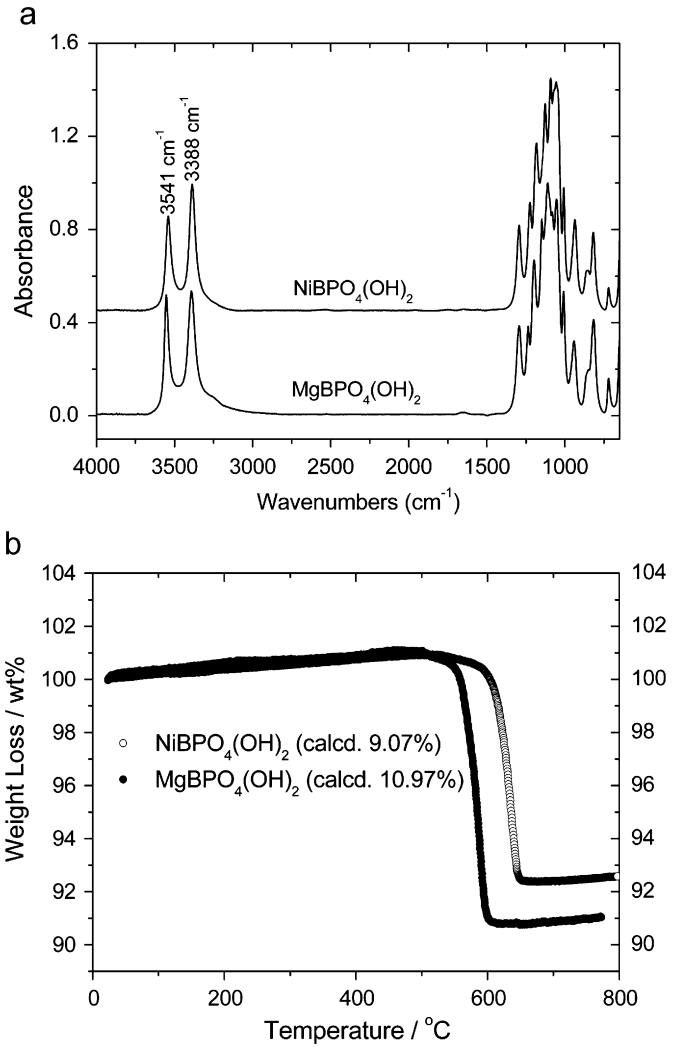

Fig. 3. (a) Two characteristic O–H vibration bands at about 3388 and 3541 cm^{-1} are present in the FT-IR spectra, which attribute to the hydroxyl groups. (b) TGA curves of $MBPO_4(OH)_2$ (M = Mg, Ni).

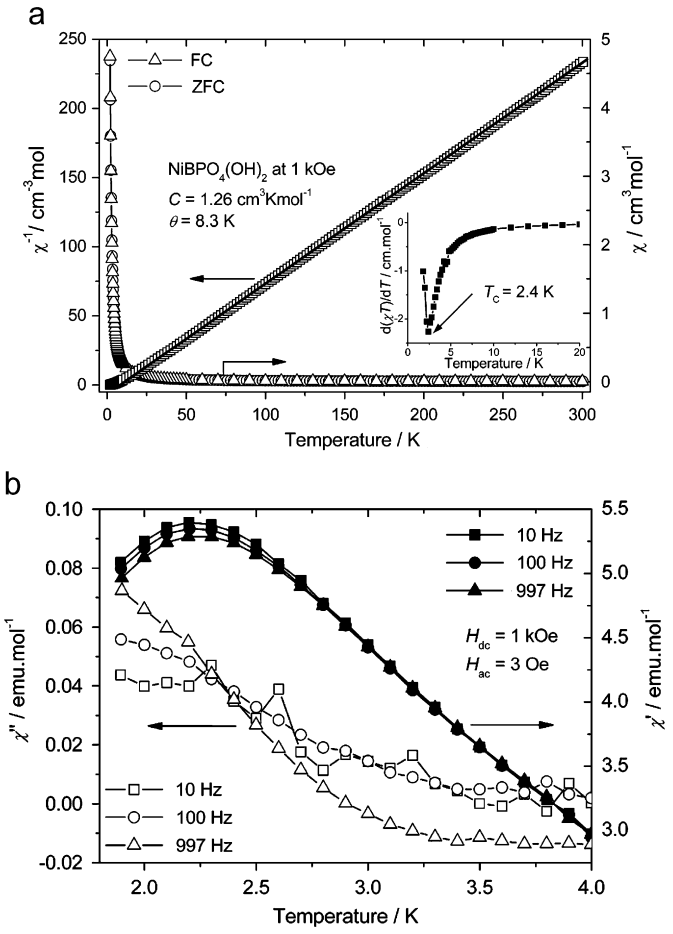

Fig. 4. (a) Temperature-dependent dc susceptibility χ and its reciprocal χ^{-1} vs. T at an external field of 1000 Oe. The inset is the $d(\chi T)/dT$ curve. (b) Temperature-dependent ac susceptibility (χ', in-phase signals; χ'', out-of-phase signals) for $NiBPO_4(OH)_2$ at frequencies of 10 (■/□), 100 (●/○) and 997 Hz (▲/□).

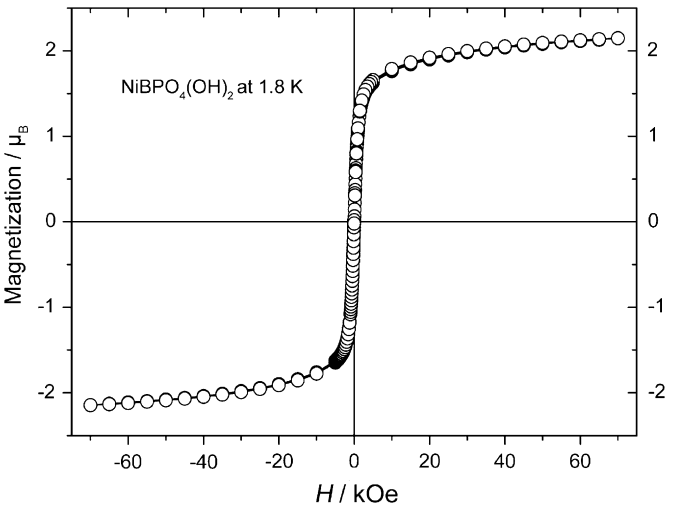

Fig. 5. Field dependence of the magnetization plot at 1.8 K for $NiBPO_4(OH)_2$.

peak at about 2.4 K (see the inset of Fig. 4a), which points to a possible long-range FM ordering. Such an ordering was then confirmed by ac susceptibility measurements between 1.9 and 4 K (see Fig. 4b). The critical temperature (T_c) was estimated to be 2.2 K from the maximum of χ' and the emergence of χ'', where χ' and χ'' are the in-phase and out-of-phase ac susceptibilities at 997–1003 oscillating field frequency range of 10–997 Hz. It is common that the estimations about the ordering temperature from dc and ac measurements are slightly deviated. The very low ordering temperature of 2.2 K is a proof that the inter-chain interactions are weak. The relatively high value of θ/T_c again reinforces our former assumption about the quasi-1D characteristic of $NiBPO_4(OH)_2$. To understand the magnetic behavior, we measured the isothermal magnetization curve at 1.8 K as shown in Fig. 5. As magnetic field increases, the magnetization quickly reaches the saturation at about 2.14 μ_B, slightly higher than the theoretical value (2 μ_B) expected from spin-only system, which is due to the orbital contribution. Since no hysteresis loop was detected, $NiBPO_4(OH)_2$ seems to be a typical soft ferromagnet or 1.8 K may not be lower enough than the long-range

ordering temperature. It is common that the coercive field and the remanent moment will increase with decreasing temperature.

4. Conclusions

In conclusion, two new borophosphates $M\mathrm{BPO_4(OH)_2}$ ($M = \mathrm{Mg}$, Ni) have been hydrothermally synthesized and the structures have been solved by powder X-ray diffraction in the space group $P3_121$. The structure comprises edge-sharing NiO_6 chains and BO_4–PO_4 vierer-single chains. Although $\mathrm{NiBPO_4(OH)_2}$ possesses a 3D framework, it can be interpreted as a quasi-1D magnet, where the intra- and inter-chain interactions are both FM, and a long-range ordering is established below 2.2 K. $M\mathrm{BPO_4(OH)_2}$ ($M = \mathrm{Mg^{2+}}$, $\mathrm{Mn^{2+}}$, $\mathrm{Fe^{2+}}$, $\mathrm{Co^{2+}}$, $\mathrm{Ni^{2+}}$) shows a good flexibility in form when crystallizing with various bivalent transition metal cations, and the coexistence of the chiral magnetic structure and the long-range ordering in $M\mathrm{BPO_4(OH)_2}$ gives a potential in searching new chiral magnetic materials with large MChD.

Acknowledgment

This work was supported by the Nature Science Foundation of China, under Contract no. 20221101.

References

[1] G.L.J.A. Rikken, E. Raupach, Nature 390 (1997) 493.
[2] R. Feyerherm, A. Loose, T. Ushida, T. Nogami, J. Kreitlow, D. Baabe, F.J. Litterst, S. Süllow, H.H. Klauss, K. Doll, Phys. Rev. B 69 (2004) 134427 and the references cited therein.
[3] E. Coronado, J.R. Galáb-Mascarós, C.J. Gómez-García, A. Murcia-Martínez, Chem. Eur. J. 12 (2006) 3484.
[4] E. Coronado, C.J. Gómez-García, A. Nuez, F.M. Romero, E. Rusanov, H. Stoeckli-Evans, Inorg. Chem. 41 (2002) 4615 and the references cited therein.
[5] R. Kniep, H. Engelhardt, C. Hauf, Chem. Mater. 10 (1998) 2930.
[6] B. Ewald, Y.X. Huang, R. Kniep, Z. Anorg. Allg. Chem. 633 (2007) 1517 and the references cited in this review.
[7] R. Kniep, H.G. Will, I. Boy, C. Röhr, Angew. Chem. Int. Ed. Engl. 36 (1997) 1013.
[8] I. Boy, R. Kniep, Z. Kristallogr. New Cryst. Struct. 216 (2001) 9.
[9] A. Baykal, M. Kizilyalli, R. Kniep, J. Mater. Sci. 35 (2000) 4621.
[10] H.Z. Shi, J.Z. Chang, H.J. Tang-Bo, H.M. Ding, Y.K. Shan, Chin. J. Chem. 24 (2006) 1255.
[11] I. Boy, R. Kniep, Z. Kristallogr. New Cryst. Struct. 216 (2001) 7.
[12] M.H. Ge, J.X. Mi, Y.X. Huang, J.T. Zhao, R. Kniep, Z. Kristallogr. New Cryst. Struct. 218 (2003) 273.
[13] I. Boy, G. Schäfer, R. Kniep, Z. Kristallogr. New Cryst. Struct. 216 (2001) 11.
[14] I. Boy, G. Schäfer, R. Kniep, Z. Kristallogr. New Cryst. Struct. 216 (2001) 13.
[15] I. Boy, F. Stowasser, G. Schäfer, R. Kniep, Chem. Eur. J. 7 (2001) 834.
[16] T. Yang, G.B. Li, J. Ju, F.H. Liao, M. Xiong, J.H. Lin, J. Solid State Chem. 179 (2006) 2534.
[17] W. Liu, Y.X. Huang, R. Cardoso, W. Schnelle, R. Kniep, Z. Anorg. Allg. Chem. 632 (2006) 2143.
[18] M. Yang, J.H. Yu, J.C. Di, J.Y. Li, P. Chen, Q.R. Fang, Y. Chen, R.R. Xu, Inorg. Chem. 45 (2006) 3588.
[19] Y. Huang, G. Schafer, W. Carrillo-Cabrera, R. Cardoso, W. Schnelle, J.T. Zhao, R. Kniep, Chem. Mater. 13 (2001) 4348.
[20] A. Yilmaz, X. By, M. Kizilyalli, G.D. Stucky, Chem. Mater. 12 (2000) 3243.
[21] S.C. Sevov, G.Y. Yang, Inorg. Chem. 40 (2001) 2214.
[22] S.C. Sevov, Angew. Chem. Int. Ed. Engl. 35 (1996) 2630.
[23] R. Kniep, G.Z. Schäfer, Anorg. Allg. Chem. 626 (2000) 141.
[24] Y.X. Huang, O. Hochrein, D. Zahn, Y. Prots, H. Borrmann, R. Kniep, Chem. Eur. J. 14 (2007) 1737.
[25] G. Schafer, H. Borrmann, R. Kniep, Z. Anorg. Allg. Chem. 627 (2001) 61.
[26] R.P. Bontchev, A.J. Jacobson, Mater. Res. Bull. 37 (2002) 1997.
[27] H.Z. Shi, M. Li, H.J. Tangbo, A.G. Kong, B. Chen, Y.K. Shan, Inorg. Chem. 44 (2005) 8179.
[28] R.P. Bontchev, J. Do, A.J. Jacobson, Inorg. Chem. 38 (1999) 2231.
[29] J. Do, L.M. Zheng, R.P. Bontchev, A.J. Jacobson, Solid State Sci. 2 (2000) 343.
[30] Y. Zhao, Z. Shi, S. Ding, N. Bai, W. Liu, Y. Zou, G. Zhu, P. Zhang, Z. Mai, W. Pang, Chem. Mater. 12 (2000) 2550.
[31] J. Do, A.J. Jacobson, Chem. Mater. 13 (2001) 2436.
[32] R.P. Bontchev, J. Do, A.J. Jacobson, Angew. Chem. Int. Ed. 38 (1999) 1937.
[33] C.J. Warren, R.C. Haushalter, D.J. Rose, J. Zubieta, Chem. Mater. 9 (1997) 2694.
[34] J. Do, R.P. Bontchev, A.J. Jacobson, Inorg. Chem. 39 (2000) 4305.
[35] C.J. Warren, R.C. Haushalter, D.J. Rose, J. Zubieta, Inorg. Chem. Commun. 1 (1998) 4.
[36] H. Engelhardt, H. Borrmann, W. Schnelle, R. Kniep, Z. Anorg. Allg. Chem. 626 (2000) 1647.
[37] R.P. Bontchev, J. Do, A.J. Jacobson, Inorg. Chem. 39 (2000) 3320.
[38] M. Asnani, A. Ramanan, J.J. Vittal, Inorg. Chem. Commun. 6 (2003) 589.
[39] Y. Wang, J. Yu, Q. Pan, Y. Du, Y. Zou, R. Xu, Inorg. Chem. 43 (2004) 559.
[40] E. Dumas, C. Debiemme-Chouvy, S.C. Sevov, J. Am. Chem. Soc. 124 (2002) 908.
[41] A. Yilmaz, X. Bu, M. Kizilyalli, R. Kniep, G.D. Stucky, J. Solid State Chem. 156 (2001) 281.
[42] M. Yang, J.H. Yu, L. Shi, P. Chen, G.H. Li, Y. Chen, R.R. Xu, Chem. Mater. 18 (2006) 476.
[43] Y.X. Huang, B. Ewald, W. Schnelle, Y. Prots, R. Kniep, Inorg. Chem. 45 (2006) 7578.
[44] C. Dong, J. Appl. Crystallogr. 32 (1999) 838.
[45] TOPAS V2.1: General Profile and Structure Analysis Software for Powder Diffraction Data, Bruker AXS, Karlsruhe, Germany.
[46] T. Yang, J. Ju, G.B. Li, S.H. Yang, J.L. Sun, F.H. Liao, J.H. Lin, J. Sasaki, N. Toyota, Inorg. Chem. 46 (2007) 2342.